Journal of
Intelligent Material
Systems and Structures

Article

Journal of Intelligent Material Systems and Structures
24(8) 962–972

DOI: 10.1177/1045389X12461076
jim.sagepub.com
SAGE

Fusion welding of nickel–titanium and 304 stainless steel tubes: Part II: tungsten inert gas welding

Gordon Fox, Ryan Hahnlen and Marcelo J Dapino

Abstract

Shape memory nickel–titanium is attractive for lightweight actuators as it can generate large blocking stresses and high recovery strains through solid-state operation. A key challenge is the integration of the nickel–titanium components into systems; this alloy is difficult and expensive to machine and challenging to weld to itself and other materials. In this research, we join nickel–titanium and 304 stainless steel tubes of 9.53 mm (0.375 in) in diameter through tungsten inert gas welding. By joining nickel–titanium to a common structural material that is easily machined and readily welded to other materials, the system integration challenges are greatly reduced. The joints prepared in this study were subjected to optical microscopic inspection, hardness mapping, energy dispersive X-ray spectroscopy, mechanical testing, and failure surface analysis via scanning electron microscopy. The affected zone from welding is approximately 125 μm (0.005 in) wide including partially mixed zones with a maximum hardness of 817 HV and a possible heat-affected zone of 1–2 μm (39–79 μin) wide. The maximum average ultimate torsional strength is 415 MPa (60.2×10^3 lbf/in^2). Implementation of this joining method is demonstrated in the construction of a solid-state torsional actuator that can lift a weight of 2.3 kg (5 lb) to a distance of 610 mm (24 in). The laser and TIG welding processes are compared.

Keywords

Shape memory alloys, NiTi, TIG welding, system integration

Introduction

Part I focused on creating and evaluating viable tubular joints between nickel–titanium (NiTi) and 304 stainless steel (304 SS) constructed through laser welding, whereas Part II focuses on creating similar NiTi/304 SS joints made through tungsten inert gas (TIG) welding. While laser welding heats and melts the base metals through the application of a focused laser beam, TIG welding utilizes an electric arc emanating from a nonconsumable tungsten electrode to heat the workpieces. With TIG welding, it is possible to join materials with a wide variety of thicknesses (Hobart Institute of Welding Technology, 2002, 2009). TIG welding is a higher-energy process than laser welding, so it is generally capable of deeper weld penetrations. It is also more common in industry than laser welding, thus leading to a lower cost for making these joints due to the possibility of using existing equipment. Despite the benefits, the heat source of TIG welders is not as finely focused as that of laser welders, which leads to larger fusion zones (FZs) and heat-affected zones (HAZ) and likely more loss of shape memory and superelastic properties when joining NiTi components.

The concerns surrounding NiTi/304 SS welds discussed in Part I, loss of cold work and training, hot and cold cracking, and affected zone width (Cieslak, 1993; Van der Eijk et al., 2003; Wang, 1997; Wu, 2001) are equally important in creating TIG welds. Hence, a similar analysis is conducted by observing intermetallic formation–based cracking, weld penetration, affected zone width, hardness, joint composition, and mechanical strength. Intermetallic formation is mitigated through the use of Ni filler metal (Hall, 2005), atmospheric contamination is avoided through the use of argon shielding gas, and the effect of heat from the joining process on NiTi is quantified via microanalysis. Three joints were created and characterized through the microanalysis via optical microscopy, hardness

Smart Materials and Structures Laboratory, Department of Mechanical and Aerospace Engineering, The Ohio State University, Columbus, OH, USA

Corresponding author:
Marcelo J Dapino, Smart Materials and Structures Laboratory, Department of Mechanical and Aerospace Engineering, The Ohio State University, Columbus, OH 43210, USA.
Email: dapino.1@osu.edu

mapping, energy dispersive X-ray spectroscopy (EDS), and mechanical strength testing. The failure surface of one of the specimens that was mechanically tested to failure was analyzed with scanning electron microscopy (SEM). Additionally, a fourth joint was made for a torsional actuator to demonstrate the ability to integrate NiTi tubes into a mechanical system using the TIG welding method developed in this study.

Experimental procedure

Sample construction

NiTi and 304 SS tubes were TIG welded together in a butt joint configuration. Both tubes have an outer diameter of 9.53 mm (0.375 in), and their inner diameters were left as received: 5.72 and 6.22 mm (0.225 and 0.245 in) for the NiTi and 304 SS tubes, respectively. This reduced the necessary preweld machining of the NiTi, which is both difficult and expensive. The three NiTi tubes for the characterization joints were cut via electrical discharge machining (EDM). The tube that was integrated into a torsional actuator was cut with an abrasive saw and then faced on a manual lathe with hand-ground high-speed steel bits. Chattering, excessive tool wear, and loss of shape memory properties were not encountered in any of these machining processes, though chattering and tool wear were a significant problem while drilling radial pinholes for fixturing the NiTi tubes that were tested mechanically. The Ni interlayer consisted of custom-made commercially pure nickel unions (Ni 200) inserted into the tubes prior to welding. Figure 1(a) shows a diagram of the weld joint and Figure 1(b) shows a photograph of a completed joint.

The welds were made using an AMI M307 power supply coupled to a M9-750 weld head, which was fitted with collets for tubes with an outer diameter of 9.53 mm (0.375 in). Prior to welding, the oxide layer on the outer surface of the NiTi tubes was removed with a tungsten carbide file. The oxide layer on the inner surface was removed with an inner diameter scraper.

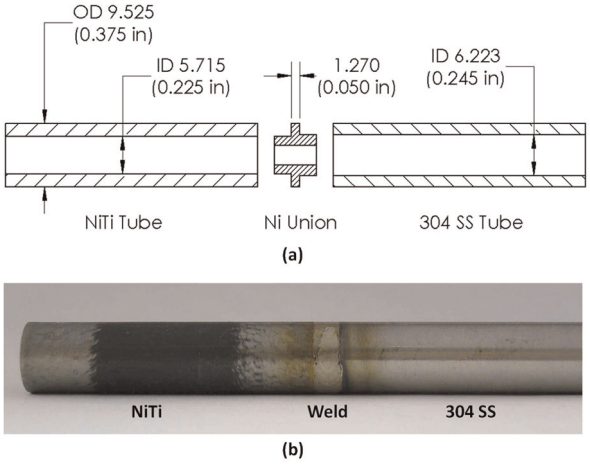

Figure 1. (a) Exploded diagram of TIG-welded specimen; (b) photograph of completed TIG weld.
TIG: tungsten inert gas.

Two different geometries of tungsten electrodes were used. For specimens 1 and 2, the electrode had a standard 22° included angle, while for specimens 3 and 4, it was 30°. Both electrodes had a diameter of 1.6 mm (1/16 in), had 0.25 mm (0.010 in) wide flats and used an arc gap of 1.1 mm (0.045 in). The duty cycles for the primary and background electric pulses were 0.19, and the background current was 21.3 A. The primary current was reduced every 90° through the orbit from 70.8 to 53.1 A to account for base metal heating. The welds were made in a single orbit, which took approximately 20 s, with a 20-s pre- and postweld argon gas purge.

Optical microscopy, hardness mapping, and EDS

NiTi/304 SS TIG weld 2 was sectioned via EDM and mounted for optical micrography. The weld penetration and general structure of the weld were obtained from the micrographs. Weld penetration was measured using the software ImageJ (US National Institutes of Health, 2009). Similar to the laser samples in Part I, possible regions include the composite weld pool or FZ, consisting of multiple partially mixed zones, as well as an unmixed zone, HAZ, and base metal.

In addition to optical observation of the weld penetration and the weld structure, a hardness map was made from specimen 2. The hardness map was created by making an array of indents with a diamond indenter and 25 g load, spaced 100 μm (0.003 in) apart in both the axial (x-axis) and radial (y-axis) directions. The map was used to determine the hardness of the bulk NiTi tube and to observe variations in hardness due to possible formation of a large-scale HAZ and intermetallic compounds. The resolution of this hardness map was not sufficient to investigate some small-scale features of the weld, so it was augmented with individual hardness tests that were conducted at points of interest.

After hardness testing was completed, the section of TIG weld 2 was analyzed for composition via EDS in regions of interest near the NiTi fusion boundary using a scanning electron microscope. By determining the composition in different regions, it is possible to determine whether optically observed regions denote a partially mixed zone, HAZ, or unmixed zone. The variation in composition is also used to account for observed variation in mechanical properties and failure locations.

Mechanical testing and failure surface analysis

Specimens 1 and 3 were strength tested to failure under a torsional load. For fixturing purposes, 3.2 mm

(1/8 in) diameter pin holes were drilled radially through each base metal 15 mm (0.6 in) from the center of the weld. The torque was measured with a strain gauge–based torque cell and the angular deflection between the sample grips was measured with an optical encoder. Deflection was applied at a rate of approximately 0.5°/s.

Similar mechanical tests were conducted on specimens made entirely out of NiTi and 304 SS to compare with the welded specimens' results. These specimens had the same geometry and fixturing as the welded specimens. Because the NiTi and 304 SS tubes had the same length as the TIG-welded specimens, their measured deflections were halved to estimate how much each material contributed to the deflection of the TIG-welded specimens. The test of the 304 SS tube gave the yield strength of the base metal to compare with the strength of the welds.

After mechanical testing, the failure surface of specimen 3 was analyzed with SEM to ascertain the failure mode. Prior to the fracture analysis, the sample was rinsed with methanol and allowed to dry at room temperature.

System integration

The fourth TIG-welded specimen was used to build a torsional actuator to demonstrate the incorporation of welded NiTi tubes into the mechanical system illustrated in Figure 2. The actuator has 304 SS tubes welded on both ends of a 150 mm (6 in) long NiTi tube. One of these 304 SS tubes is fixtured rigidly, while the one on the other end of the NiTi tube is supported with ball bearings to allow it to rotate when the NiTi tube twists. An additional ball bearing supports the middle of the NiTi tube to prevent torsional buckling. A gear is attached to the freely rotating 304 SS tube, which meshes with a smaller gear on a shaft connected to a pulley. A weight of 2.3 kg (5 lb) is suspended from a wire rope on this pulley, providing a torque to the NiTi tube. The NiTi tube was trained to have a two-way shape memory effect prior to welding, so it twists approximately 120° in one direction when heated and returns when cooled, regardless of whether a torque is applied to it or not. It is heated by an electrical resistance cartridge heater located inside the tube and cooled by convection from an external fan.

Results and discussion

Optical microscopy

An optical micrograph of specimen 2 is shown in Figure 3. The weld penetrates through 1.32 mm of 1.90 mm (0.052 in of 0.075 in) wall thickness of the NiTi tube. In between the most prominent region of the weld pool and the bulk NiTi at the left of the picture, a light

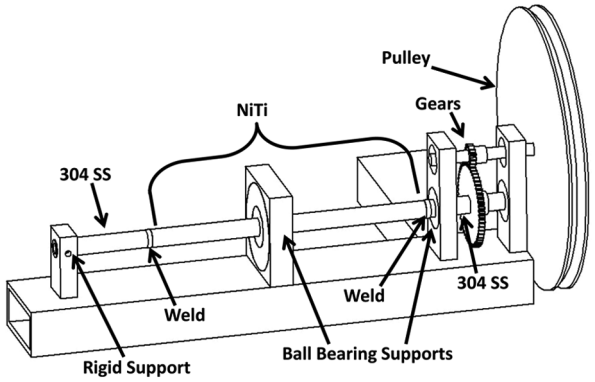

Figure 2. Illustration of shape memory torsional actuator.

shaded region is observed. This region is 125 μm (49.2×10^{-4} in) wide and follows the contour of the fusion boundary, then continues toward the center of the tube between the unmelted NiTi and Ni union. In this region, the molten weld metal was likely drawn between the NiTi tube and Ni union through capillary action. The total affected zone is believed to consist of one or more partially mixed zones, possibly an unmixed zone, and the NiTi HAZ. The region between the NiTi FZ and NiTi tube was studied more in depth than the region between the 304 SS FZ and the 304 SS tube because that is where the welds failed during mechanical testing, and where defects in the weld were most likely to form.

Within the affected zone, there is a secondary region that is shown in Figure 3(b). This second region is very narrow and has an irregular boundary with the main affected zone. This region appears to consist of a homogeneous compound, and the irregular boundary with the main affected zone represents solidification nucleation sites of this region, indicating it was liquid at some point in the welding process. Figure 3(b) also shows a very narrow region directly between the secondary affected zone and the bulk NiTi. We believe that this region is either an optical manifestation of the HAZ or an unmixed region where the bulk NiTi became liquid but solidified before mixing with the rest of the weld pool (Tillack, 1993). These observations place the NiTi fusion boundary of the weld either immediately to the left of the secondary affected zone or the narrow region.

Two cracks can be observed in the micrograph. These cracks, which are located between the NiTi tube and the nickel union, are believed to have been formed due to the presence of intermetallic compounds. Evidence for this hypothesis is supported by the EDS analysis discussed in the following sections. It is unclear whether similar defects were present in the mechanically tested samples. However, the similarity of strength between the two mechanically tested samples, as discussed later, suggests that if such cracks were present,

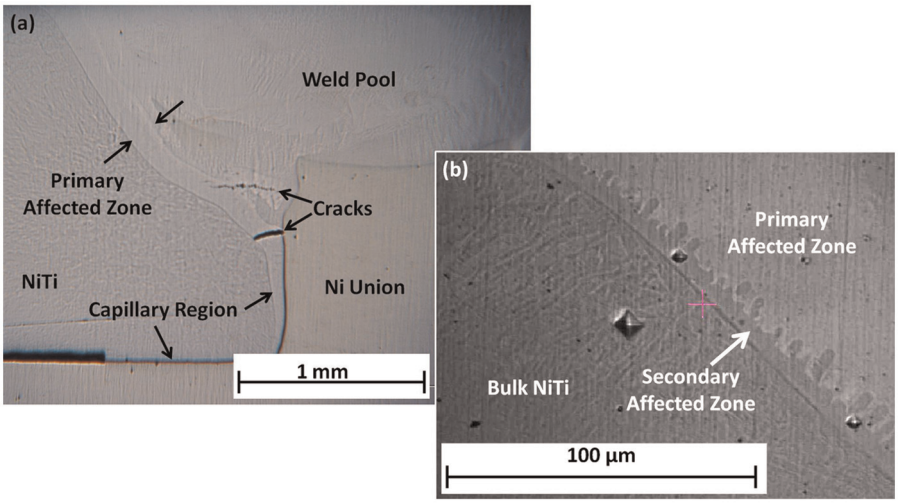

Figure 3. Micrograph of (a) NiTi/304 SS weld 2 and (b) affected zone of NiTi/304 SS weld 2.

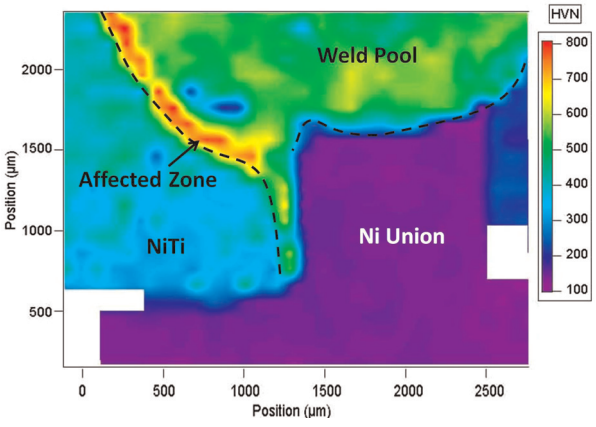

Figure 4. Hardness map of NiTi/304 SS weld 2 showing Vickers hardness number (HVN). The dotted line shows the approximate location of fusion boundaries.

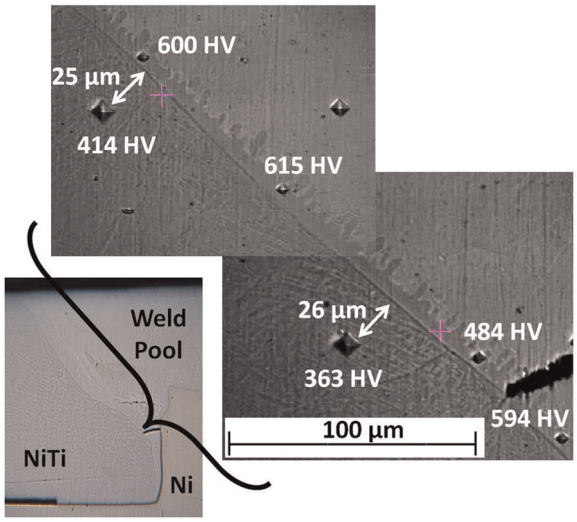

Figure 5. Hardness in the secondary affected zone of NiTi/304 SS weld 2.

they did not cause much variation in the strength of the welds.

Hardness mapping

The hardness map of specimen 2 is shown in Figure 4. NiTi far from the weld pool has hardness between 200 and 400 HV, which is typical for NiTi (Alapati et al., 2006) and indicates that the thermomechanical properties have not been altered in this region. To the right of the fusion boundary, there is a region of increased hardness, up to 817 HV. This region corresponds to the lighter region observed in optical micrographs, such as Figure 3(a). As the increases in hardness are within the NiTi FZ, it is assumed that the loss of shape memory properties in the unmelted NiTi tube is limited to regions with hardness values less than that of the bulk NiTi. However, lack of a widespread HAZ indicates that there is little loss of the shape memory effect in the NiTi outside the FZ due to changes in grain structure from the heat generated during welding.

Hardness measurements in the larger primary affected zone were observed through the hardness map, but individual hardness tests were needed to measure the smaller secondary region because it is narrower than the space between indents in the hardness map. Figure 5 shows that this region has individual hardness values ranging from 484 to 615 HV, significantly harder than the bulk NiTi but softer than the main affected zone. The cause for the increased hardness of both regions is further discussed in the following section.

Two indents in the NiTi taken at 25 and 26 µm (9.4 and 10.2 $\times$ 10^{-4} in) from the affected zone boundary have hardness values of 414 and 363 HV, respectively. This further puts a bound of approximately 25 µm on the width of the possible overall HAZ in the

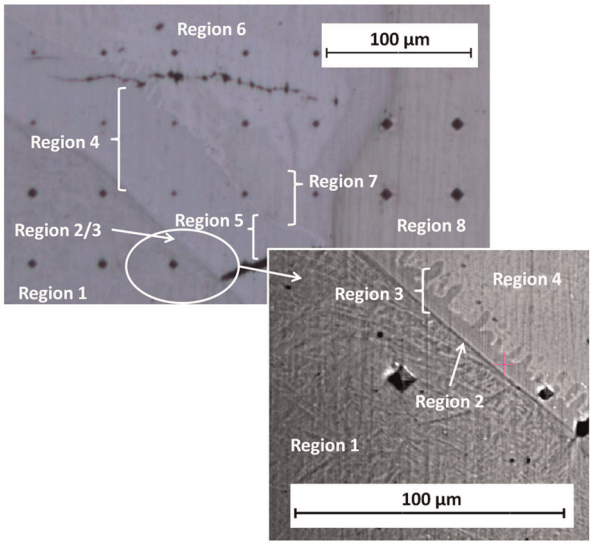

Figure 6. Regions identified in NiTi/304 SS weld 2.

NiTi as these regions do not show the decrease in hardness typically associated with a NiTi HAZ (Falvo et al., 2005; Tam et al., 2011).

The resolution of the hardness map is too coarse to provide information about the capillary region observed between the unmelted NiTi and nickel union, so additional individual hardness data points were taken to investigate it. The hardness of the capillary region was found to range from 557 to 597 HV, which is harder than the bulk NiTi and similar to the hardness of the secondary affected zone.

Through microscopy and hardness testing, the identified affected zone was found to be small relative to both the thickness of the weld and overall tube length. Since the hardness of the NiTi piece returns to typical values for nonjoined NiTi very close to the observed fusion boundary, it is likely that any loss of cold work, shape memory, or superelastic properties is limited to the NiTi consumed by the weld in the FZ. However, the increased hardness observed in this region indicates that it is a likely location for weld failure, as discussed in the following sections.

EDS analysis

Through optical microscopy and SEM, eight distinct regions were observed as the sample transitions from bulk NiTi to the weld pool, as shown in Figure 6. The nature of these regions, whether they represent part of the base metal, a HAZ, unmixed zone, or partially mixed zone, is determined through region morphology and composition. The composition of each region except for region 2 was determined through EDS analysis, as shown in Table 1. Region 2 is excluded because it is only 1–2 μm wide along the entire NiTi boundary, which is smaller than the estimated interaction volume of the electron beam used for the composition analysis.

Through the composition analysis, region 1 is found to be similar in composition to the bulk NiTi tube. Furthermore, the hardness map and individual hardness studies indicate that material in this region is unaffected by the welding. While region 2 was not able to be analyzed either through EDS or hardness testing, its location and size are similar to the possible HAZ or unmixed regions observed in the laser samples discussed in Part I. For this reason, region 2 is hypothesized to be either part of the HAZ or the unmixed zone of the TIG-welded samples. If region 2 is indeed the HAZ, it is very small compared with the HAZ reported in the literature for laser welds between NiTi wires (Falvo et al., 2005; Tam et al., 2011). Similar to Part I, this difference is believed to be due to the fact that small-scale welds have less material for heat dissipation, while comparatively large tubes adjacent to the TIG welds allow for more heat absorption from the weld without the development of high temperatures in the base metal. In addition to a larger amount of material, the relatively small HAZ is attributed to the preferential heat flow through the 304 SS tube rather than the NiTi piece due to the differences in thermal conductivity of NiTi, Ni 200, and 304 SS (Johnson Matthey, 2011; McGuire, 2008; Mankins and Lamb, 1990). The narrow width of this region, especially compared to regions 3 and 4, indicates that the orbital TIG process does not significantly affect the NiTi tube via HAZ formation, and as such, there should be little loss of trained behavior due

Table 1. Composition of bulk base metals and transition regions in NiTi/304 SS TIG sample 2, as seen in Figure 6.

Analysis region	Ni (at%)	Ti (at%)	Fe (at%)	Mn (at%)	Cr (at%)
Bulk NiTi	50.8	49.2	—	—	—
Bulk 304 SS	9.3	—	69.1	1.4	20.2
Region 1	50.3	49.7	—	—	—
Region 3	57.3	42.7	—	—	—
Region 4	61.7	38.3	—	—	—
Region 5	62.9	36.0	1.2	—	—
Region 6	72.1	24.9	2.1	0.5	0.4
Region 7	85.3	13.7	1.0	—	—
Region 8	100.0	—	—	—	—

TIG: tungsten inert gas.

to excessive heating of the shape memory alloy. The loss of shape memory or superelastic properties could be estimated by the amount of NiTi consumed in the FZ of the weld. In the FZ, alloying with the filler or opposite base metal alters the composition of the NiTi base metal, either changing or eliminating the shape memory or superelastic properties. Further study is required to observe the crystalline structure of the material in region 2 to confirm the presence of the HAZ in this area as well as measure its size. The attempts to etch the weld section for this purpose were hindered by the composite nature of the weld as the solution preferentially etched the Ni filler material and did not reveal grain structure in either of the base metals.

Regions 3 and 4 were previously observed in optical microscopy studies. Region 3 has a composition of 57.3 at% Ni and 42.7 at% Ti, resulting in a Ni-to-Ti ratio of 1.34. A likely compound for this region is Ni_4Ti_3, which would result in a Ni-to-Ti ratio of 1.33. The increased Ni content of region 3 indicates that it was formed due to mixing of liquid phases of the NiTi tube and Ni filler, indicating region 3 is a partially mixed zone. The irregular boundaries between regions 3 and 4 and regions 4 and 6 indicate that region 4 was liquid at some point during weld formation. The composition of region 4 is 61.7 at% Ni and 38.3 at% Ti with a Ni-to-Ti ratio of 1.61, suggesting a composition of Ni_3Ti_2, which has a Ni-to-Ti ratio of 1.5, in solid solution with Ni from the filler metal to account for the increased Ni content. Due to the irregular boundary and increased Ni content, region 4 is most likely a partially mixed zone distinct from region 3 and the rest of the weld pool. Both Ni_4Ti_3 and Ni_3Ti_2 are intermetallic compounds (Li et al., 2000; Saburi et al., 1986), which provide an explanation for the increased hardness in the optically identified fusion regions and may act as potential failure locations during mechanical loading. Analysis of the capillary region between the inner diameter of the NiTi tube and Ni union revealed compositions similar to regions 3 and 4. This is further proof that these regions were in a liquid phase during welding as the weld did not penetrate to the inner diameter of the NiTi tube. This would require that regions 3 and 4 flowed into the space between the NiTi tube and Ni union, as opposed to forming locally due to mixing or temperature-induced diffusion.

Region 5 appears to be a mixing region of partially mixed zones associated with the Ni union and NiTi tube. It appears in an approximately triangular region bound by regions 4 and 7 as well as the crack observed in Figures 3 and 6. The primary difference in composition between regions 4 and 5 is the inclusion of 1.2 at% Fe in region 5. This may allow for the formation of Ti–Fe intermetallics in addition to the Ni–Ti intermetallics likely present in region 4. No hardness indents had been made in this region as it was not readily visible in optical micrographs.

Region 6 is ubiquitous within and has no discernible boundary with the weld pool. It is thus believed to be a compositional constituent of the weld pool. As seen in Table 1, it is the only tested region to contain all constituent elements present in the 304 SS base metal. Indents made in region 6 show that it has a nominal hardness of 550 HV. Hardness values observed in the weld pool range from 500 to 600 HV with isolated regions of low hardness, reinforcing that region 6 is one of the most prevalent compounds in the weld pool.

Region 7 is adjacent to both the weld pool and the remaining solid Ni union, region 8. For this reason, it is assumed to be a partially mixed zone associated with the Ni union. This is supported by the high Ni content (85.3 at%) observed in this region. Both the Fe and Ti contents in this region allow for the formation of Ni–Ti and Ti–Fe intermetallics, which may contribute to the moderately increased hardness in this region, approximately 500 HV. The presence of such intermetallics may also account for the formation of the crack seen in Figures 3 and 6, which appears to originate and terminate in regions 3 and 7. Both of these regions are believed to have possible intermetallic formation as well as increased hardness relative to the bulk materials that may have contributed to the crack formation.

Mechanical testing

Specimens 1 and 3 were tested in torsion to failure and broke at the interface between the weld pool and the NiTi tube, likely in the affected zone comprising regions 3 and 4. Their ultimate torques are listed in Table 2, and a photograph of a broken weld is shown in Figure 7. The ultimate torques are consistent between the two samples, only differing by 2%, which indicates that this TIG welding process can produce consistent joints.

Since there is only partial weld penetration and a capillary region with unknown bonding properties, calculations of the shear stress in the joints are more difficult than for a homogeneous material. The material in this capillary region may act as a braze joint, allowing stress transfer from the NiTi tube to the nickel union, or it may transmit no stress at all. To give a range of the strengths of the welds, ultimate shear stresses are calculated using three different assumptions. The first assumption is that the capillary region transmits no stress, so the inner radius, r_i, used to calculate the polar

Table 2. Ultimate torque of TIG-welded specimens.

Specimen	Ultimate torque, N m (in lb)
1	52.1 (458)
3	51.0 (448)
Average	51.6 (453)

TIG: tungsten inert gas.

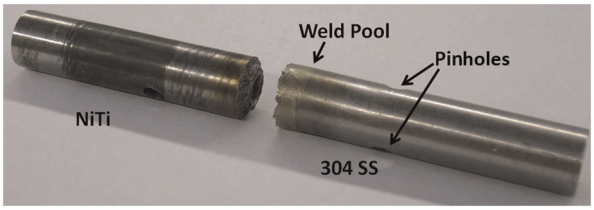

Figure 7. NiTi/304 SS weld after strength testing.

Table 3. Ultimate shear strength of TIG-welded specimens.

Specimen	Ultimate shear strength, τ, MPa (10^3 lbf/in^s)		
	Case 1 Weld r_i	Case 2 NiTi r_i	Case 3 Ni r_i
1	419 (60.8)	350 (50.8)	317 (46.0)
3	410 (59.5)	343 (49.7)	310 (45.0)
Average	415 (60.2)	347 (50.3)	314 (45.5)

TIG: tungsten inert gas.

moment of inertia for the shear stress calculation is the inner radius of the bottom of the weld penetration, 3.44 mm (0.135 in). The second assumption is that the capillary region transmits stress directly through the butt end of the NiTi tube to the nickel union, so the inner radius is that of the NiTi tube, 2.86 mm (0.113 in). The last assumption is that the capillary region transmits stress through the entire contacting area of the NiTi tube and nickel union, so the inner radius of the nickel union is used, 2.10 mm (0.083 in). The resulting ultimate shear stresses for each assumption are tabulated in Table 3.

A plot of the torque as a function of the angle of twist of the specimen grips is shown in Figure 8. There are three main regions: an initial linear-elastic region, the NiTi detwinning region, and a mixed deformation region, which includes elastic deformation of the detwinned NiTi tube and plastic deformation of the 304 SS tube. Due to the thick walls of the specimens, the material on the inner and outer surfaces experiences significantly different shear stresses at a given torque. This means that the onset of detwinning in the NiTi tube and yielding in the 304 SS tube occurs over a range of torques, which is unlike tension tests where each of these occurs at a discrete load. This makes changes in the slope of the torque versus angle plot at the start of detwinning and yielding rounder and less defined than in plots of tensile load versus deformation. The fact that the stress is not uniform across the cross section of the tube, unlike uniaxial tension tests, makes the detwinning region stiffer in torsion than in simple tension. This effect was also observed in torsional tests of tubes with a similar geometry by Sun and Li (2002).

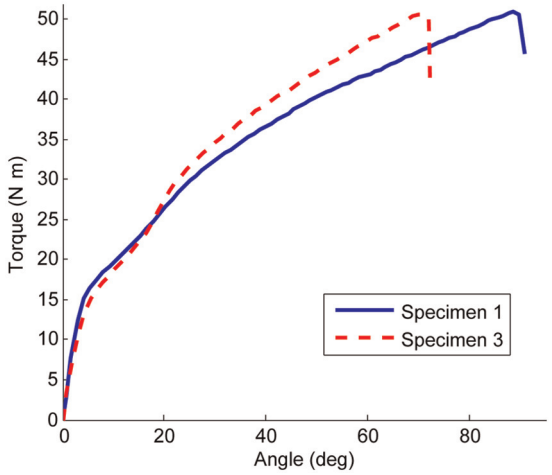

Figure 8. Torque versus angle from NiTi/304 SS weld mechanical test.

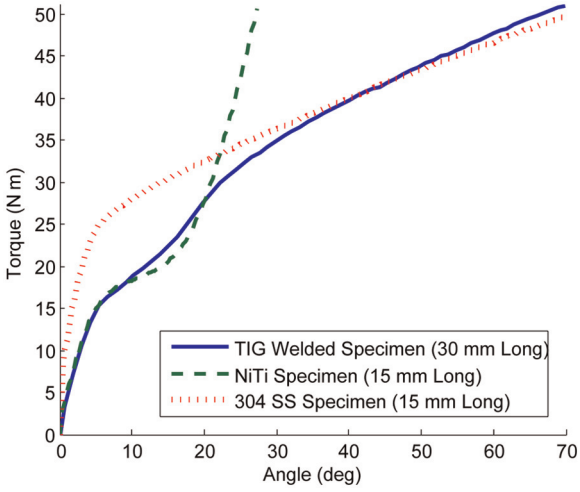

Figure 9. Torque versus angle of TIG-welded specimen 1 and unwelded base metals.
TIG: tungsten inert gas.

The torque versus angle curve of TIG-welded specimen 1 is compared to that of unwelded NiTi and 304 SS tubes in Figure 9. This comparison helps identify the detwinning and plastic deformation regions in Figure 8. From the plots of the welded specimens and NiTi tube, it can be seen that the initial linear region ends and detwinning starts at around 15.9 N m (140 in lb). This corresponds to a shear stress of 107 MPa (15.5 10^3 lbf/in^s) in the outer material of the NiTi tube. The start of detwinning occur at similar torques in the welded specimens and in the NiTi tube but the welded specimens require greater stress to continue detwinning, which correlates with the findings of Falvo et al. (2005) on laser-welded NiTi. The critical detwinning stresses are shown in Table 4. The onset of plastic deformation in

Table 4. TIG-welded specimen and unwelded NiTi tube critical torques and stresses.

Specimen	Critical start torque, N m (in lb)	Critical finish torque, N m (in lb)	Critical start stress, MPa (10^3 lbf/in^s)	Critical finish stress, MPa (10^3 lbf/in^s)
TIG weld 1	14.7 (129)	22.9 (201)	98.8 (14.3)	154 (22.4)
NiTi tube	16.6 (146)	21.2 (186)	111 (16.2)	143 (20.7)

TIG: tungsten inert gas.

the 304 SS tube around 26.2 N m (230 in lb) coincides with the torque where the deformation of the welded specimen started deviating significantly from that of the NiTi tube. Because the NiTi tube was stiffer after detwinning than the plastically deforming 304 SS tube, most of the deflection of the welded specimen in the mixed deformation region in Figure 8 is due to yielding of the 304 SS tubes, not the NiTi tubes. Yielding was not encountered in the NiTi tubes before 51.2 N m (450 in lb), so it can be concluded that the NiTi in the welded specimens did not yield before the welds failed.

The stainless steel used in this study was annealed, and the outer material started to yield at a torque of about 26.2 N m (230 in lb), which is close to the end of the detwinning region observed in the unwelded NiTi tube. This is undesirable for mechanisms using these welds because NiTi cannot be fully detwinned without starting to yield the connected 304 SS tubes. However, the strength of 304 SS tubes can be increased via heat treatment and cold work to be greater than the strength of these welds (Mangonon and Thomas, 1970). Changing the geometry of the 304 SS piece welded to the NiTi tubes cannot increase the strength of the joints much by itself. If solid rods were used instead of tubes, the strength would only increase by 20%. This means that a solid 304 SS rod would start to yield at 31.4 N m (275 in lb), which is still not safely more than the torque necessary to detwin all of the NiTi tube.

Failure surface analysis

In mechanical testing, failure of the welds occurred between the weld pool and NiTi tube, as seen in Figure 7, closely following the fusion boundary observed in optical microscopy of weld 2. This suggests that the formation of intermetallic compounds observed in the partially mixed zones is the likely cause of failure. The sudden failure indicates brittle failure at the macroscopic level. Unaided observations of the fracture surface reveal several faceted reflective regions that indicate brittle failure at the microscopic level as well (Mills and Davis, 1987).

SEM images of the fracture surface of weld 3 are shown in Figure 10. The bottom right image indicates the direction of rotation with the large arrow at the bottom. The first feature observed is several cracks oriented at approximately 45° from the axis of rotation. The position of these cracks suggests that they were caused by mode I fracture aligned perpendicular to the direction of maximum tensile stress in the weld, a characteristic of brittle fracture (Becker, 2002). As magnification is increased, the most prominent features are larger areas of smooth surfaces and river patterns. Both of these are indicative of transgranular fracture. These features are characteristic of cleavage, a brittle mode of fracture. Cracks are also ubiquitous at higher magnifications and further support the brittle nature of microscopic failure as brittle materials dissipate energy through the creation of new surfaces (Mills and Davis, 1987). While cleavage is the main morphology observed in the surface, there are isolated instances of dimples that are formed through microvoid coalescence. The primarily brittle failure morphology is consistent with the previous findings for welded NiTi (Yan et al., 2006).

System integration

The solid-state torsional actuator is able to lift the weight suspended from it when heated and lower it when cooled. Once the cartridge heater inside the NiTi tube is turned on, it takes about 30 s to heat it above the austenite finish temperature. When it is turned off, the NiTi tube takes about 5 min to cool below its martensite finish temperature by free convection. The cooling process can be sped up with cooling fans, so that it takes 2 min for the heated tube to return to its martensite configuration. The NiTi tube lifts a weight of 22 N (5 lb) a distance of 610 mm (24 in) when actuated, which is shown in Figure 11. A video of the actuator can be seen at http://www.mecheng.osu.edu/smsl/project-videos.

The torque on the NiTi tube and welds is calculated by $T = P \times r \times n$, where T is the torque, P is the weight, r is the pulley radius, and n is the gear ratio. For this actuator, $P = 22$ N (5 lb), $r = 76$ mm (3 in) and $n = 4$, so the NiTi tube is subjected to 6.8 N m (60 in lb) of torque. This torque corresponds to a shear stress in the outer material of the NiTi tube of 46 MPa (6.7 10^3 lbf/in^s). Although this torque is much less than the welds can withstand, the design of the 304 SS/gear attachment limits the allowable torque. The work done by the actuator in this case is 13 J.

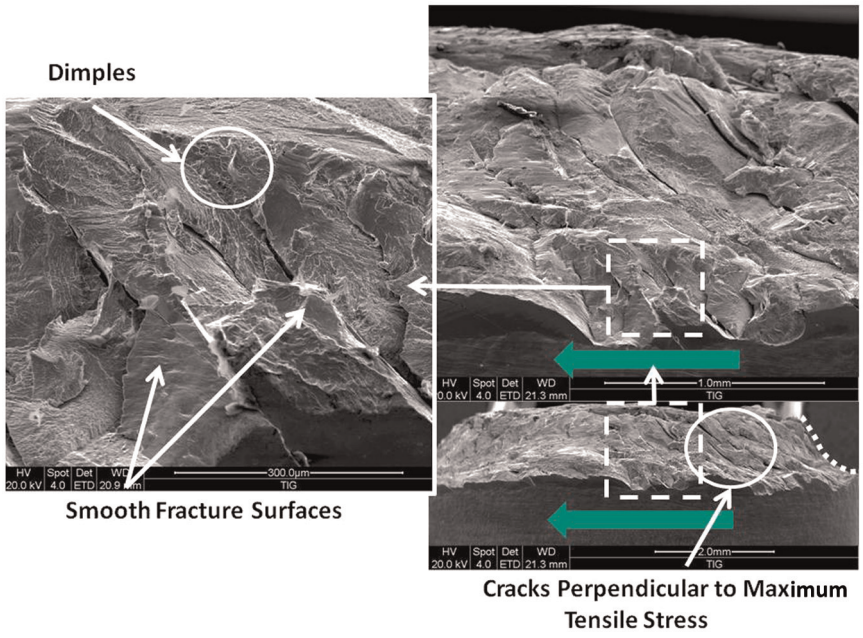

Figure 10. SEM image of the NiTi failure surface showing cracks "perpendicular to" the direction of principal tensile stresses. The large arrows show the direction in which the shear load was applied; the dotted lines illustrate fracture profiles.

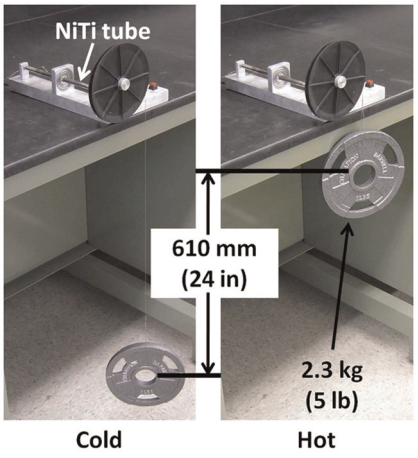

Figure 11. Torsional actuator before and after heating.

Conclusion

TIG welding conclusions

The TIG welding process was utilized to make butt joints between tubes with an OD of 9.5 mm (0.375 in). The NiTi tubes had a wall thickness of 1.90 mm (0.075 in), and the 304 SS tubes had a wall thickness 1.65 mm (0.065 in). Three samples were created for weld characterization. Of these, one tube was sectioned for microanalysis including optical microscopy, hardness mapping, and composition analysis via EDS, while the other two were mechanically tested until failure. From the mechanically tested welds, the fracture surface of specimen 3 was analyzed to determine the nature of the weld failure.

Although two small cracks were observed in the optical micrograph of the sectioned weld, there was no large-scale cracking and the welds were able to withstand a shear stress larger than the yield strength of the annealed 304 SS. This indicates that there was sufficient Ni filler metal present in the weld to prevent immediate failure due to Ti–Fe intermetallic formation, thus allowing the creation of viable joints between NiTi and 304 SS.

Through optical microscopy, an affected zone 125 μm (0.005 in) wide was observed in the TIG welds. Within this region, two subregions could be identified. These regions were further characterized through hardness mapping and individual hardness testing and were found to be partially mixed zones contiguous with the fusion boundary. Mapping showed that all hardness changes, and hence detrimental effects on the shape memory properties of the NiTi tube, are limited to the optically observed partially mixed zones within the weld pool. The prominent partially mixed zone, region 4, had a maximum hardness of 817 HV, while the lesser partially mixed zone, region 3, had a maximum hardness of 615 HV, both of which are significantly harder than bulk NiTi.

The composition analysis via EDS revealed that the two primary partially mixed zones observed in optical microscopy are likely composed of Ni–Ti intermetallic compounds, Ni_4Ti_3 and Ni_3Ti_2. The presence of these compounds explains the observed increase in hardness

and correlates with the observed failure site in mechanical testing. While performing EDS, a region 1–2 μm wide was observed. Based on the laser welds studied in Part I, it is believed that this small region is either an unmixed zone or possibly the HAZ for the TIG welds. If this region is not the HAZ, individual hardness measurements indicate that the HAZ does not extend beyond 25 μm from the fusion boundary.

The ultimate torque of these welds was 52 N m (450 in lb), which corresponds to a shear strength between 315 and 415 MPa (45 and 60 10^3 lbf/in^s), depending on the properties of a region observed in the micrographs below the weld penetration. The strength of the welds is greater than the yield strength of the annealed 304 SS. While the beginning of the detwinning region was observed in torque–angle plots, the end of the detwinning plateau was obscured by plastic deformation of the 304 SS. For design of an actuator that would take full advantage of the shape memory properties of NiTi, the 304 SS would need to be strengthened. The analysis of the fracture surface of sample 3 revealed that the specimen failed in a brittle mode at the microscale through transgranular fracture. Furthermore, the fracture surface profile appears similar to the fusion boundaries observed in optical micrographs indicating that intermetallic compounds within the partially mixed zones are the likely cause of failure.

A solid-state torsional actuator was designed and constructed using the TIG welding procedure presented. The actuator is capable of lifting a weight of 2.3 kg (5 lb) a distance of 610 mm (24 in). The actuator generates up to 6.8 N m (60 in lb) of torque and has a maximum work output of 13 J.

In this research, we have studied two different fusion welding methods for joining NiTi and 304 SS tubes. The results show that laser (Part I) and TIG (Part II) welding are viable processes for joining NiTi to 304 SS for use in solid-state actuators. The process affects only a small amount of the joined NiTi and, with the addition of Ni filler metal, prevents cold cracking due to the widespread formation of intermetallic compounds. The resulting strength of the joints is high enough to allow for the generation of blocking forces or strain recovery and is not the limiting factor in the joint systems that were studied.

Laser welding and TIG welding comparison

Both Part I and Part II of this research focus on joining shape memory NiTi to 304 SS and characterizing the resulting system. In both cases, it is shown that Ti–Fe intermetallic formation that has hindered NiTi fusion welding can be mitigated through the use of a nickel filler metal. Many current commercial uses for NiTi are applicable to small diameter NiTi wires and thin sheets. Laser welding is an appropriate joining method as the focused nature of the heat source affects very little of the material outside the immediate weld region. However, this benefit comes at the expense of practical weld depth, on the order of a few millimeters. The large blocking stresses that NiTi can generate are applicable to large-scale applications as well, but as actuator geometry increases, weld penetration must increase as well.

In Part I, we were able to create a butt joint between NiTi and 304 SS with a depth of 1.65 mm (0.065 in) using a double bevel geometry that essentially allows an unlimited joint depth. While arbitrary depth welds can be made with laser welding, multiple passes must be made which in turn require a longer amount of time needed to complete each joint. In Part II, TIG welding was used to create a similar NiTi/304 SS butt joint with a depth of 1.32 mm (0.052 in) in a single pass procedure. While slightly smaller in penetration, the TIG weld procedure could be adjusted to give a comparable depth joint in a single pass thus providing a significant time savings.

While the TIG process may produce welds more quickly, much more heat is applied to the joint during welding. This is easily observed in comparing the affected zones, consisting primarily of intermetallics containing partially mixed zones, between the laser and TIG samples. Thin-walled single pass laser samples exhibits a total affected zone width of 7.90 μm (3.11×10^{-4} in), while the multipass thick-walled samples have an average affected zone width of 21.9 μm (8.62×10^{-4} in). In comparison, the TIG weld sections exhibit an affected zone width of 125 μm (49.2×10^{-4} in), over a five-fold increase in width. From the EDS analysis, the different intermetallic compounds formed in the partially mixed zones for each joining method were identified. While both the thick-walled laser and TIG samples have one partially mixed zone likely consisting of Ni_3Ti_2, the thick-walled laser sample has an additional partially mixed zone likely consisting of Ni_3Ti and the additional partially mixed zone in the TIG sample likely consists of Ni_4Ti_3. All three of these compounds are intermetallics and are found at the observed failure sites; however, the exact effects of one compound over the other are unknown. From a strength and reliability perspective, reducing the size of these regions is a concern. Under this metric, laser welding is the better option for minimizing the intermetallic containing partially mixed zone present in both joining methods.

The altering of the base metal through the formation of a HAZ effectively causes a loss of shape memory properties; thus, a smaller HAZ is desirable. In both laser and TIG samples, no large-scale HAZ was observed in hardness testing, believed to be due to preferential heat flow through the 304 SS portion of the joints. A greater loss of shape memory properties is through the consumption of the base metal within the FZ, including the identified partially mixed zones, as mixing with the Ni filler alters the composition of the NiTi, effectively creating a new alloy with unknown properties. Any design using either fusion welding

technique would have to account for the base material consumed by the weld pool when considering total actuator deflections and effective actuator length.

In mechanical testing, the thick-walled laser sample had an ultimate shear strength of 346 MPa (50.2 10^3lbf/in^s) while the average ultimate shear strength of the TIG welds falls between 314 and 415 MPa (45.5 and 60.2$\times10^3$lbf/in^2) depending upon the nature of the capillary region. Thin-walled laser samples are excluded from this comparison as to avoid effects of shear distribution differences arising from different NiTi wall thicknesses. For this initial strength study, it appears that both laser and TIG welds have similar stresses; however, further study is necessary due to the small sample size.

While this two part study found that laser and TIG welding are both capable of producing NiTi/304 SS joints of similar geometry and strength, the benefit of one process over the other must be determined on a case-by-case basis. Laser welding is best suited for shallow welds; however, we have demonstrated the ability to make arbitrary depth joints using multiple welding passes. The result is a joint that has a very narrow affected zone at the expense of weld time. In contrast, TIG welding can create deeper welds in a single pass, but this process results in an affected zone that is over five times larger.

Funding

This research is funded by the member organizations of the Smart Vehicle Concepts Center (www.SmartVehicleCenter.org), a National Science Foundation Industry/University Cooperative Research Center (I/UCRC). The work of R.H. was supported in part by a Smart Vehicle Concepts Center Graduate Fellowship.

Acknowledgements

The authors thank Tim Frech and Steve Manring from the Edison Welding Institute for their assistance in preparing the samples, Suresh Babu and Tapasvi Lolla from the Ohio State University Materials Science and Engineering Department for assistance with the hardness measurements, and Jim Mabe and Tad Calkins from the Boeing Company for their technical support.

References

Alapati S, Brantley W, Nusstein J, et al. (2006) Vickers hardness investigation of work-hardening in used NiTi rotary instruments. *Journal of Endodontics* 32: 1191–1193.

Becker WT (2002) *ASM Handbook: Volume 11—Failure Analysis and Prevention*. Materials Park, OH: ASM International.

Cieslak MJ (1993) *ASM Handbook: Volume 6—Welding, Brazing, and Soldering*. Materials Park, OH: ASM International.

Falvo A, Furgiuele F and Maletta C (2005) Laser welding of a NiTi alloy: mechanical and shape memory behaviour. *Materials Science and Engineering A—Structural Materials: Properties, Microstructure and Processing* 412: 235–240.

Hall P (2005) *Method of welding titanium and titanium based alloys to ferrous metals*. US Patent No. 6875949.

Hobart Institute of Welding Technology (2002) *Gas Tungsten Arc Welding*. Troy, OH: Hobart Institute of Welding Technology.

Hobart Institute of Welding Technology (2009) *Welding Guide*. Troy, OH: Hobart Institute of Welding Technology.

Johnson M (2011) *Nitinol Technical Specifications: Transformation, Physical, Electrical, Magnetic and Mechanical*. Available at: http://jmmedical.com

Li B, Rong L, Li Y, et al. (2000) Fabrication of cellular Ni–Ti intermetallic compounds. *Journal of Materials Research* 15(1): 10–13.

McGuire MF (2008) *Stainless Steels for Design Engineers*. Materials Park, OH: ASM International.

Mangonon P and Thomas G (1970) Structure and properties of thermal-mechanically treated 304 stainless steel. *Metallurgical and Materials Transactions B - Process Metallurgy and Materials Processing Science* 1(6): 1587–1594.

Mankins WL and Lamb S (1990) *ASM Handbook: Volume 2—Properties and Selection: Nonferrous Alloys and Special-Purpose Materials*. Materials Park, OH: ASM International.

Mills K and Davis JR (1987) *ASM Handbook: Volume 12—Fractography*. Materials Park, OH: ASM International.

Saburi T, Nenno S and Fukuda T (1986) Crystal structure and morphology of metastable X Phase in shape memory Ti–Ni alloys. *Journal of the Less-Common Metals* 125: 157–166.

Sun Q-P and Li Z-Q (2002) Phase transformation in superelastic NiTi polycrystalline micro-tubes under tension and torsion from localization to homogeneous deformation. *International Journal of Solids and Structures* 39(13–14): 3797–3809.

Tam B, Khan MI and Zhou Y (2011) Mechanical and functional properties of laser-welded Ti–55.8 Wt Pct Ni nitinol wires. *Metallurgical and Materials Transaction A—Physical Metallurgy and Materials Science* 42: 2166–2175.

Tillack DJ (1993) Nickel, Nickel-Copper, Nickel-Chromium, and Nickel-Chromium-Iron Alloys. *ASM Handbook: Volume 6—Welding, Brazing, and Soldering*. Materials Park, OH: ASM International, pp. 586–592.

US National Institutes of Health (2009) ImageJ. Available at: http://rsbweb.nih.gov/ij

Van der Eijk C, Fostervoll H, Sallom Z, et al. (2003) Plasma welding of NiTi to NiTi, stainless steel and Hastelloy C276. In: *Proceedings of ASM materials solutions*, Pittsburgh, PA, 13-15 October, 2003.

Wang G (1997) Welding of nitinol to stainless steel. In: *Proceedings of the international conference on shape memory and super elastic technologies, SMST-97,* (ed A Pelton, D Hodgson, S Russell, T Duerig), Pacific Grove, CA, 2-6 March, 1997, pp. 131–136.

Wu M (2001) Fabrication of nitinol materials and components. In: *Proceedings of the international conference on shape memory and super elastic technologies* (ed Y.Y Chu and L.C Zhao), Kunming, China, 2-6 September, 2001, pp. 258–292. Trans Tech Publications Inc. Dumtem-Zurich.

Yan XJ, Yang DZ and Qi M (2006) Rotary-bending fatigue of a laser-welded superelastic NiTi alloy wire. *Materials Characterization* 57(1): 58–63.